Eur Biophys J (2011) 40:1043–1060
DOI 10.1007/s00249-011-0721-4

ORIGINAL PAPER

Transverse and tangential orientation of predicted transmembrane fragments 4 and 10 from the human multidrug resistance protein (hMRP1/ABCC1) in membrane mimics

Béatrice de Foresta · Michel Vincent · Manuel Garrigos · Jacques Gallay

Received: 29 March 2011 / Revised: 23 May 2011 / Accepted: 1 June 2011 / Published online: 24 June 2011

Abstract The human multidrug-resistance-associated protein 1 (hMRP1/ABCC1) belongs to the large ATP-binding cassette transporter superfamily. In normal tissues, hMRP1 is involved in tissue defense, whereas, in cancer cells, it is overproduced and contributes to resistance to chemotherapy. We previously investigated the folding properties of the predicted transmembrane fragments (TM) TM16, and TM17 from membrane-spanning domain 2 (MSD2). These TMs folded only partially as an α-helix and were located in the polar headgroup region of detergent micelles used as membrane mimics (Vincent et al. in Biochim Biophys Acta 1768:538–552, 2007; de Foresta et al. in Biochim Biophys Acta 1798:401–414, 2010). We have now extended these studies to TM4 and TM10, from MSD0 and MSD1, respectively. TM10 may be involved in the substrate translocation pathway whereas the role of TM4 is less predictable, because few studies have focused on MSD0, a domain present in some hMRP1 homologs only. Each TM contained a single Trp residue (W142 or W553) acting as an intrinsic fluorescent probe. The location and dynamics of the TMs in dodecylphosphocholine (DPC) or *n*-dodecyl-β-D-maltoside (DDM) micelles were studied by Trp steady-state and time-resolved fluorescence, including quenching experiments. Overall TM structure was analyzed by far-UV circular dichroism studies in detergent micelles and TFE. TM10 behaved similarly to TM16 and TM17, with an interfacial location in micelles consistent with a possible role in lining the transport pore. By contrast, TM4 behaved like a classical TM fragment with a high α-helical content, and its transmembrane insertion did not require its interaction with other TMs.

Keywords Multidrug-resistance · ABCC1 · Transmembrane fragment · Fluorescence · Circular dichroism · Detergent micelles

Abbreviations

hMRP1 (or ABCC1)	Human multidrug-resistance protein 1
BCRP (or ABCG2)	Breast cancer-resistance protein
LTC_4	Cysteinyl leukotriene C_4
$E_2 17\beta G$	Estradiol 17-(β-D-glucuronide)
GSH	Reduced glutathione
DDM	*n*-dodecyl-β-D-maltoside
BrDDM (BrDM in our previous papers)	7,8-Dibromododecylmaltoside
BrUM	10,11-Dibromoundecanoyl-maltoside
DPC	Dodecylphosphocholine
Cmc	Critical micellar concentration
NATA	*N*-acetyltryptophanamide
TOE	Tryptophan octyl ester
DMSO	Dimethylsulfoxide

Electronic supplementary material The online version of this article (doi:10.1007/s00249-011-0721-4) contains supplementary material, which is available to authorized users.

B. de Foresta (✉) · M. Garrigos
CEA, iBiTecS, Service de Bioénergétique Biologie Structurale et Mécanismes, 91191 Gif-sur-Yvette, France
e-mail: beatrice.de-foresta@cea.fr

B. de Foresta · M. Garrigos
CNRS, URA 2096, 91191 Gif-sur-Yvette, France

M. Vincent · J. Gallay (✉)
Institut de Biochimie et Biophysique Moléculaire et Cellulaire, Université Paris-Sud 11, UMR 8619, Bât. 430, Orsay, France
e-mail: jacques.gallay@u-psud.fr

M. Vincent · J. Gallay
CNRS, UMR 8619, Orsay, France

TFE	Trifluoroethanol
TFA	Trifluoroacetic acid
MSD	Membrane-spanning domain
TM	Transmembrane fragment
NBD	Nucleotide-binding domain
MEM	Maximum entropy method
CD	Circular dichroism
FWHM	Full width at half maximum
P3	$K_2WL_9AL_9K_2A$
P5	$K_2CLWL_7AL_9K_2A$
P7	$K_2CL_3WL_5AL_9K_2A$
P9	$K_2CL_5WL_3AL_9K_2A$
P11	$K_2CL_7WLAL_9K_2A$
P13	$K_2CL_9WL_9K_2A$
TM16	A_{1195}NRWLAVRLECVGNCIV-LFAALFAV$_{1219}$
mTM16	A_{1195}NRWLAVRLESVGNSIV-LFAALFAV$_{1219}$
TM17	A_{1227}GLVGLSVSYSLQVT-TYLNWLVRMS$_{1251}$
mTM17	K_{1227}GLVGLSVSYSLQVT-TYLNWLVRMS$_{1251}$
TM4	V_{132}QSSGIMLTFWLVAL-VCALAILRSK$_{156}$
mTM4	V_{132}QSSGIMLTFWLV-ALVSALAILRSK$_{156}$
TM10	S_{546}AVGTFTWVCTPFL-VALCTFAVYVT$_{570}$
mTM10	S_{546}AVGTFTWVSTP-FLVALSTFAVYVT$_{570}$
	(all synthetic peptides were Ac– and –Am)

Introduction

The 49 human ATP-binding cassette (ABC) transporters constitute the largest family of integral membrane proteins and are involved in various physiological processes involving the ATP-dependent translocation of endogenous compounds and xenobiotics across intracellular membranes or out of the cell (Holland and Blight 1999; Holland et al. 2003). On the basis of sequence and structural analyses, the 49 ABC transporters have been classified into seven subfamilies of proteins: ABCA through ABCG (Dean and Allikmets 2001). The human multidrug-resistance-associated protein 1 (hMRP1/ABCC1) was discovered in 1992 (Cole et al. 1992) and was the first member of the ABCC subfamily, which has 13 members: ABCC1 through ABCC13 (http://nutrigene.4t.com/humanabc.htm), although the ABCC13 gene is thought to be a pseudogene that does not encode a functional protein. The ABCC subfamily includes 10 transporters MRP1–10 (ABCC1–6 and ABCC10–13) together with a chloride channel (CFTR/ABCC7) and the sulfonylurea receptors (SUR1-2/ABCC8-9), which regulate a potassium channel. Mutations in four genes encoding ABCC proteins have been implicated in genetic diseases (Dubin-Johnson syndrome (ABCC2), Pseudoxanthoma elasticum (ABCC6), cystic fibrosis (ABCC7), and persistent hypoglycemia of infancy (ABCC8) (Borst and Elferink 2002; Flanagan et al. 2007)). The various MRPs have varied physiological functions, which can be predicted on the basis of their levels of expression, cellular location, and the nature of the compound transported. hMRP1 is expressed constitutively at moderate levels in most healthy tissues and is capable of transporting a wide range of structurally unrelated molecules, including amphiphilic anionic conjugates, for example glutathione (GSH)-conjugated, glucuronate-conjugated, and sulfate-conjugated aliphatic or heterocyclic compounds, across membranes (Cole and Deeley 2006; Deeley and Cole 2006; Deeley et al. 2006). hMRP1 also transports unconjugated drugs in the presence of GSH, probably through a cotransport mechanism (Borst et al. 2006; Cole and Deeley 2006; Grant et al. 2008; Loe et al. 1996; Rappa et al. 1997; Rothnie et al. 2008). Together with the P-glycoprotein (P-gp or ABCB1) (Ambudkar et al. 2003) and the breast cancer-resistance protein BCRP (ABCG2/MXR) (Robey et al. 2009), hMRP1 and most of its homologs are, to different extents, associated with the multidrug-resistance phenotype (MDR) (Haimeur et al. 2004; Leslie et al. 2005; Marquez and Van Bambeke; Sharom 2008). hMRP1 is strongly expressed in many drug-resistant solid tumors and is probably a major obstacle to successful chemotherapy in lung cancer (Deeley et al. 2006). Moreover, it has recently been shown that the overexpression of hMRP1 in patients with primary ovarian cancer is an adverse marker for outcome and cancer aggressiveness (Faggad et al. 2009). However, despite extensive studies, the use of various transporter modulators in clinical trials for cancer has proved disappointing to date (Fletcher et al. 2010). Finally, the fact that substances of toxicological relevance are transported by hMRP1 and that this protein is expressed constitutively in biological barriers, for example the blood–brain barrier, suggests possible involvement in defense against xenobiotics. The other MRPs may vary substantially in their distribution in polarized tissues and substrate specificity, reflecting differences in physiological functions (Liu et al. 2010).

According to protein folding algorithms, hMRP1 (GenBank™ accession number: P33527) contains three membrane-spanning domains (MSD). The current topological model (Scheme 1), which is supported by epitope insertion (Kast and Gros 1997, 1998) and glycosylation site mutation data (Hipfner et al. 1997), includes a specific N-terminal domain, MSD0, preceded by an extracytosolic N-terminus

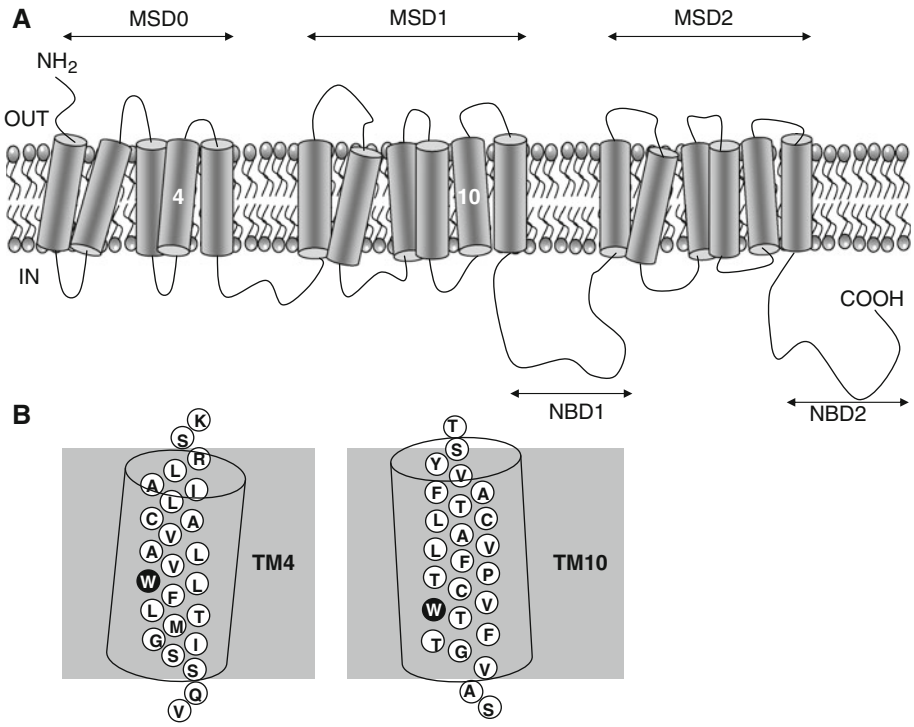

Scheme 1 Topology of hMRP1 membrane transporter. **a** membrane insertion model of the whole transporter **b** isolated putative TM4 and TM10 with highlighted Trp residues

and followed by a cytosolic loop (L0), together with two membrane domains, MSD1 and MSD2, each followed by a nucleotide-binding domain (NBD). Five transmembrane (TM1-5) helices are predicted for MSD0, whereas MSD1 and MSD2 each consist of six TM fragments, numbered TM6–11 and TM12–17, respectively. This topology, MSD0–MSD1–NBD1–MSD2–NBD2, is also displayed by ABCC2, ABCC3, ABCC6 and ABCC8–10. All other known human ABC full transporters lack the MSD0 domain (Tusnady et al. 2006).

However, the length of the predicted extracytosolic N-terminal segment is variable and the corresponding sequences are not well conserved (Yang et al. 2002), accounting in part for the differences in the functional relevance of MSD0 in ABCC homologs. For example, MSD0 is essential for the function of ABCC8 as a channel regulator (Babenko and Bryan 2003; Chan et al. 2003). By contrast, a truncated human ABCC1 from which MSD0 has been deleted is able to transport LTC4 and is correctly targeted to the plasma membrane (Bakos et al. 1998). However, if the C-terminal part of ABCC1 is modified by mutation, MSD0 becomes essential for protein trafficking (Westlake et al. 2005). Moreover, it has recently been suggested that about 32 amino acids from the extracytosolic N-terminal end of the protein form a U-shaped structure that functions as a gate (Chen et al. 2006).

High-resolution crystal structures were initially determined for ABC transporters from various prokaryotes (Hollenstein et al. 2007). Two of these transporters were exporters, similar to hMRP1: the bacterial lipid transporter MsbA (Ward et al. 2007) and the Sav1866 transporter from *S. aureus* (Dawson and Locher 2006, 2007), both crystallized in various conformations (recently reviewed by Kerr et al. 2010). Models of hMRP1 MSD1, and MSD2 have been proposed on the basis of these structures (DeGorter et al. 2008 and references cited therein). For eukaryotic ABC transporters, an X-ray structure of mouse P-gp in an inward-facing conformation was recently determined at a resolution of 3.8 Å, revealing the presence of a large internal cavity for drug-binding (Aller et al. 2009). For hMRP1, a 3D density map has been constructed from data obtained by electron cryomicroscopy of 2D crystals and this may suggest that there is extensive contact between MSD0 and the core domains, MSD1 and MSD2 (Rosenberg et al. 2010). However, in the absence of a high-resolution crystal structure for hMRP1, complementary biophysical approaches remain informative. Investigation of the structural properties of membrane proteins by study of isolated transmembrane (TM) fragments is a widely recognized approach (Hunt et al. 1997; Rath et al. 2009). This approach is based on a two-stage model (Popot and Engelman 1990, 2000) that emerged from early studies of bacteriorhodopsin refolding (Liao et al. 1983), according to which the folding of membrane proteins includes an initial step in which independently stable transmembrane helices are formed, this step being followed by the association of these helices within the membrane. A more comprehensive view includes additional stages, for example helix–helix association, leading to further folding events (Engelman et al. 2003). Initial events, for example the interfacial

binding and folding of a TM fragment, have also been rationalized thermodynamically (White and Wimley 1999). The way in which proteins are inserted into membranes in vivo, by interaction with the translocon, is also becoming clearer (Bernsel et al. 2008; Lundin et al. 2008) and recent progress in studies of membrane protein folding has been reviewed (Bowie 2005; Fiedler et al. 2010).

We previously studied the hMRP1 TM16 and TM17 fragments (and their Trp variants) from MSD2 (de Foresta et al. 2010; Vincent et al. 2007) because mutagenesis studies showed that both these fragments contained polar and ionizable amino acids important for the transport function of the protein (Ito et al. 2001; Situ et al. 2004; Zhang et al. 2002). According to molecular modeling (DeGorter et al. 2008), these fragments are part of the transmembrane pore. Moreover, they each also contain a single Trp residue that could be used as a fluorescent reporter. Our experimental results for Trp fluorescence and circular dichroism (CD), with detergent micelles as membrane mimics, were consistent with these TMs being located close to the surface of the mixed peptide-detergent complexes. These fragments were only partly structured into α-helices. These TM characteristics are consistent with these fragments lining the hydrophilic transport pore.

In this work, we extended this approach to two other fragments from the other two membrane-spanning domains: TM4 from MSD0 and TM10 from MSD1. TM4 is the only predicted fragment from MSD0 containing a single Trp residue. As MSD0 is probably not directly involved in the transport pore, we hypothesized that its TM characteristics might differ from those previously described for TM16 and TM17. TM10 is also the only predicted TM fragment from MSD1 with a single Trp residue. The functional importance of TM10 has been demonstrated by photolabeling with an analog of glutathione (Karwatsky et al. 2003) and by mutagenesis studies. Mutations resulting in the replacement of two of its threonine residues (T550A and T556A) modulated the drug-resistance profile of hMRP1 and a mutation affecting the tyrosine residue (Y568A) reduced the affinity of hMRP1 for $E_2 17\beta G$ (Zhang et al. 2006). In addition, mutations affecting the single proline (P557A) or the single Trp (W553A) residue decreased the transport of various organic anion substrates (Koike et al. 2002, 2004).

The isolated TMs were obtained by chemical synthesis and their sequences are shown in Table 1. According to the topological model (Scheme 1), their N-termini face the intracellular space and their C-termini face the extracellular space in the folded protein. Mutations were introduced to convert Cys residues into Ser residues, to prevent the formation of disulfide bonds. The TMs were then studied in dodecylphosphocholine (DPC) and dodecylmaltoside (DDM) micelles and mixed micelles of DDM with two brominated analogs of DDM described elsewhere (de Foresta et al. 1996, 1999). These non-ionic detergents were chosen as appropriate membrane mimics, as previously discussed (de Foresta et al. 2010; Vincent et al. 2007 and references cited therein). We can, in particular, emphasize that they form optically clear systems wherein scattering artifacts in the UV range are minimized compared with lipid vesicles. In addition, because of the highly dynamic properties of the micelles, a thermodynamic equilibrium with peptides can be rapidly obtained (Bordag and Keller 2010). We also used TFE (or mixed TFE–water), a solvent known to promote the formation of α-helical structures (Buck 1998). The binding and location of peptides in micelles, and Trp environment and dynamics were studied by steady-state and time-resolved fluorescence spectroscopy, including Trp quenching with acrylamide and the two brominated analogs of DDM (de Foresta et al. 1996, 1999). The secondary structure of the TMs was analyzed by far-UV circular dichroism studies. Striking differences in insertion behavior and structure were found between TM4 and TM10 in membrane mimics. These differences can be interpreted on the basis of differences in the functional roles of TMs and the recently reported low-resolution structure of hMRP1 (Rosenberg et al. 2010).

Table 1 Sequences of the 25-amino acid synthetic peptides with their corresponding wild-type TMs from hMRP1

Peptide name	Amino acid sequence	Charge	ΔG_u^a (kcal/mol)
TM4	V_{132}QSSGIMLT**FW$_{142}$**LVALVC_{148}ALAILRSK_{156}	++	−5.78
mTM4[b]	Ac-V_{132}QSSGIMLT**FW$_{142}$**LVALVS_{148}ALAILRSK_{156}-Am	++	−5.41
TM10	S_{546}AVGT**F**T**W$_{553}$**VC_{555}TP**F**LVALC$_{563}$T**F**AV**Y**VT_{570}	0	−8.18
mTM10[b]	Ac-S_{546}AVGT**F**T**W$_{553}$**VS_{555}TP**F**LVALS$_{563}$T**F**AV**Y**VT_{570}-Am	0	−7.44

The residues are numbered as in hMRP1. All three aromatic amino acids are shown in bold characters

[a] Interfacial partitioning free energy for unstructured peptide, calculated with MPEX 3.0, for partitioning from water to the bilayer, for the N-terminal-acetylated and C-terminal-amidated peptide

[b] From the 21 amino acid sequences predicted for hMRP1 (from Swissprot-Uniprot-hMRP1, code P33527) to which were added the two N-terminal and C-terminal amino acids of the same sequence. Mutations introduced: C_{148}S in mTM4, C_{555}S and C_{563}S in mTM10

Materials and methods

Chemicals

We obtained *n*-dodecyl-β-D-maltoside (DDM) from Calbiochem. Its brominated derivatives 7,8-dibromododecylmaltoside (BrDDM) and 10,11-dibromoundecanoylmaltoside (BrUM) were synthesized by Insavalor (Villeurbanne, France), as previously described (de Foresta et al. 1996, 1999). DPC was obtained from Anatrace (OH, USA). Stock solutions of these detergents were prepared in Milli-Q water, at concentrations of 100 or 200 mM. *N*-Acetyltryptophanamide (NATA) and acrylamide were purchased from Sigma–Aldrich. We prepared a stock solution of 5 M acrylamide in water. 2,2,2-Trifluoroethanol (TFE) (for synthesis) was obtained from Merck. Buffers were filtered through Millex-HA filters (0.45 μm pore size; Millipore).

Peptide synthesis

Two 25-amino acid peptides were synthesized as trifluoroacetate salts by Jerini (Berlin, Germany), as shown in Table 1:

1. a peptide referred to as mTM4 (Mw = 2745), encompassing predicted transmembrane fragment 4 of hMRP1 but with replacement of the native Cys148 residue by a Ser residue (amino-acid sequence numbering corresponds to the full-length published sequence of human MRP1); and
2. a peptide referred to as mTM10 (Mw = 2706), encompassing predicted transmembrane fragment 10 of hMRP1, but with replacement of the native Cys555 and Cys563 residues by Ser residues.

These peptides were acetylated at the N-terminus and amidated at the C-terminus. They were delivered at a purity of 85–90%, according to matrix-assisted laser desorption ionization time-of-flight (MALDI/TOF) mass spectrometry or HPLC–MS. These peptides were freeze-dried and stored at −20°C, and were used as supplied.

Peptide solubilization in solvent and detergent micelles

The hydrophobic nature of TM fragments makes them difficult to handle and great care must be taken to avoid their aggregation. As for TM16 and TM17 (de Foresta et al. 2010), 1 (or 2) mM peptide stock solutions were prepared in TFE, an α-helix-promoting organic solvent. mTM4 dissolved instantaneously in TFE, whereas vortex mixing and an equilibration period of ~30 min were required for solubilization of mTM10.

Peptide concentrations were estimated from the absorption spectra in TFE, at 20°C, using molar absorption coefficients at ~278–280 nm (ε_{max}) of 5,600 M^{-1} cm^{-1} and 7,000 M^{-1} cm^{-1} for mTM4 and mTM10, respectively, based on the absorption coefficients determined for Trp and Tyr model compounds in aqueous solutions (Pace et al. 1995). TFE only resulted in a small (1–2 nm) blue shift of the absorption spectra, as determined by comparison of the spectra of NATA in TFE and water, and the spectra of mTM4 in TFE and 4 mM DPC in buffer (not shown). The concentrations were consistent, to within ~15%, with those based on weight measurements.

Unless otherwise stated, the mixed peptide-detergent micelles were prepared by adding an aliquot of the peptide stock solution to 10 mM potassium phosphate buffer, pH 7.5, at 20°C, supplemented with 4 mM detergent (DDM, DPC, or mixtures of DDM with BrDDM or BrUM), with a dilution factor of 100–200. The average number of peptides per micelle was calculated from peptide to detergent concentrations in the different experiments, taking into account two characteristics of the detergent, the cmc and the aggregation number *N*. For each detergent:

$$[c]_m = ([c]_{det} - cmc)/N$$

where $[c]_m$ and $[c]_{det}$ are, respectively, the micelle and detergent molar concentrations. Cmc values used were 170–180, 220, and 320 μM for DDM, BrDDM, and BrUM, respectively (de Foresta et al. 1999; Møller and le Maire 1993) and 1.1 mM for DPC (Lauterwein et al. 1979). Under our usual experimental conditions, $[c]_{det}$ is 4 mM, so that $[c]_m$ ~ 30 μM and ~50 μM for DDM ($N = 125$; Tortech et al. 2001) or DPC ($N = 55$; Tortech et al. 2001), respectively. Therefore, in most experiments, with peptide concentration of 5 or 10 μM, there is much less than one peptide per micelle, and self-association is unlikely.

Absorption measurements

Absorption spectra were recorded on an HP8453 diode-array spectrophotometer with a thermostatically controlled sample holder (20°C). The sample was continuously stirred in a cuvette with a path length of 1 cm.

Steady-state fluorescence measurements

Fluorescence data were obtained with a Spex Fluorolog spectrofluorimeter under the control of the Spex DM3000F spectroscopy computer. The temperature in the cuvette was controlled with a thermostat and the sample was stirred continuously. We used standard quartz cuvettes (1×1 cm^2). Emission spectra were corrected for fluctuations in lamp intensity (usually very small, <1%) by operating in the ratio mode, in which the fluorescence signal was automatically divided by the exciting beam intensity measured by a reference photodiode.

Fluorescence quenching by acrylamide

Fluorescence was quenched with acrylamide, as previously described (Tortech et al. 2001). Peptide quenching was analyzed by use of the classical Stern–Volmer equation (reviewed by Eftink 1991):

$$F_0/F = 1 + K_{sv}[Q]$$

where F_0 and F are, respectively, the fluorescence intensities in the absence and presence of quencher, K_{sv} is the Stern–Volmer quenching constant, and $[Q]$ is the quencher concentration. K_{sv} is related to the bimolecular quenching constant k_q by the formula:

$$K_{sv} = k_q \tau_0$$

where τ_0 is the lifetime of the fluorophore in the absence of quencher.

In our case, intensity decays are multiexponential, so τ_0 was replaced by the intensity average lifetime $\langle\tau\rangle_i$, as suggested by Sillen and Engelborghs (1998). For NATA, taken as a reference, we used the nonlinear Stern–Volmer equation:

$$F_0/F = (1 + K_{sv}[Q])\exp(V[Q])$$

where V may be regarded as a sphere of action around the fluorophore in which the presence of a quencher molecule results in instantaneous (static) quenching.

Fluorescence quenching by brominated detergents

Assessments of the quenching of hMRP1 fragment fluorescence in mixed micelles of DDM with a brominated analog (BrDDM or BrUM) were performed essentially as previously described (de Foresta et al. 2002; Vincent et al. 2007). Data were analyzed with a lattice model of quenching (East and Lee 1982; London and Feigenson 1981; see also Powl et al. 2005). This model was originally designed to describe the quenching of membrane fluorophores (e.g. protein Trp) by spin-labeled or brominated phospholipids. It considers two populations of fluorophores: one completely inaccessible to the quencher and responsible for the residual fluorescence F_{min} (e.g. Trp embedded in a protein) and one in which each fluorophore has n neighbors (phospholipids) and for which fluorescence is completely quenched if at least one of these sites is occupied by a modified phospholipid (corresponding to a quenching efficiency of 100% upon contact). It is thought that phospholipids do not change position during the lifetime of the fluorophore. If X is the molar fraction of quenchers in the membrane, then $(1 - X)^n$ is the probability that none of the n sites is occupied by a quencher. The fluorescence ratio is therefore given by: $F/F_0 = (1 - F_{min}/F_0)(1 - X)^n + F_{min}/F_0$. In a micellar environment, unlike lipid bilayers, the "lattice parameter" n is not expected to enable exact determination of quenchers around Trp because, in addition to static quenching, some dynamic quenching occurs (de Foresta et al. 1999, 2002), and because the transverse inaccessibility of Trp is not taken into account directly in the model. n is, however, correlated with the accessibility of this residue to brominated alkyl chains. We used a set of six model peptides Pn with Trp at different positions in the sequence (positions 3, 5, 7, 9 and 13 in the 25-amino acid sequence) to establish calibration curves for n (de Foresta et al. 2002). We used these data as a reference, for comparison with the results obtained.

Time-resolved fluorescence

Fluorescence intensity and anisotropy decay were measured by the time-correlated single-photon counting technique from the polarized $I_{vv}(t)$ and $I_{vh}(t)$ components. These measurements were carried out as previously described for the TM16 and TM17 fragments (de Foresta et al. 2010), unless otherwise stated. Briefly, a light-emitting diode (PLS 290, serial number PLS-8-2-421 from Picoquant, Berlin-Adlershof, Germany) (maximum emission at 290 nm) working at 10 MHz was used as an excitation source and a Hamamatsu photomultiplier (model R3235-01) was used for detection. LED emission, focused with a UV lens, was filtered through a short-pass Asahi Spectra UV filter ZUS300. The fluorescence emitted was collected through a 306AELP Omega long-pass filter and a UG11 Schott broad-band glass filter. The instrument response function was obtained at the excitation wavelength, with a glycogen scattering solution. As previously described, fluorescence intensity $I(t)$ and anisotropy decays $r(t)$ were analyzed as sums of 150 or 100 exponential terms, respectively, by the maximum entropy method (MEM) (Livesey and Brochon 1987; Vincent et al. 1988; Vincent and Gallay 1991) according to the equations:

$$I(t) = \sum_i \alpha_i \exp(-t/\tau_i)$$

where α_i is the normalized amplitude and τ_i the excited state lifetime, and

$$r(t) = \sum_i \beta_i \exp(-t/\theta_i)$$

where β_i is the anisotropy and θ_i the rotational correlation time. In this analysis, we assume that each lifetime τ_i is associated with all rotational correlation times θ_i. The main advantage of MEM is that it does not impose any particular number of significant parameters for the decay. Skilling–Jaynes entropy maximization was subjected to a χ^2 constraint, to ensure consistency of the recovered distributions with the data.

Circular dichroism

Far-UV circular dichroism spectra were recorded on a Jobin–Yvon CD6 spectrodichrograph calibrated with ammonium d-10 camphorsulfonate. For measurements in TFE, we used a peptide concentration of 100 μM in a cuvette with a 0.01 cm path-length (Hellma). For measurements in detergent, the peptide concentration was 20 μM in 10 mM potassium phosphate buffer, pH 7.5, supplemented with 4 mM detergent, and a quartz cuvette with a path-length of 0.1 cm was used. Spectra were recorded at 20°C in the 185–250 (or 260) nm wavelength range, with 0.5 nm wavelength increments, a 2 nm spectral bandwidth, and an integration time of 2 s. Spectra were averaged over six scans and corrected for background. Unsmoothed spectra are presented. For comparisons of the effect of DDM, BrDDM, and BrUM on mTM4 spectra, the measurements conditions were modified slightly to improve the resolution, as indicated in the legend to Fig. 6. The CD units used are the mean residue ellipticity (MRE or $[\theta]$), expressed in degrees square centimeter per decimol of residue (deg cm^2 $dmol^{-1}$) and were calculated from:

$$[\theta] = (100\theta_m)/(ClN)$$

where θ_m is the measured ellipticity in degrees, C is the concentration in moles per liter, l is the path length of the cell in centimeters, and N is the number of residues (Chenal et al. 2009).

Secondary structure was analyzed with the Dichroweb web server (http://dichroweb.cryst.bbk.ac.uk/html/home.shtml) (Whitmore and Wallace 2004, 2008). Two different methods for analyzing protein CD spectra (CONTIN/LL for Fig. 5 and CDSSTR for Fig. 6, the latter method requiring data up to 260 nm) were used, with reference protein set 6. The quality of the results were judged by the NRMSD (normalized root-mean-square deviation) values, a goodness-of-fit variable, and comparisons of the calculated and experimental spectra. Note, however, that a low NRMSD is a necessary but not sufficient condition for an accurate result.

Results

Steady-state fluorescence spectra of mTM4 and mTM10 in various media

We first examined the binding of mTM4 to DDM and DPC micelles in phosphate buffer (pH 7.5) (online Fig. I), from the resulting fluorescence changes of its single Trp (W142) that reflect changes in the microenvironment of this residue. In the absence of detergent, Trp fluorescence intensity decreased with time and intensity fluctuations became significant, reflecting aggregation of the peptide, as previously reported for other TMs. With DPC, these effects were progressively reversed with increasing detergent concentration and the final fluorescence intensity was strongly enhanced, reflecting peptide insertion into DPC micelles. With DDM, intensity fluctuations did not completely disappear and the final fluorescence intensity was only slightly enhanced. Thus, DDM solubilizes mTM4 oligomers less efficiently than DPC. Therefore, all subsequent experiments in the presence of detergent were performed after directly adding TM4 and TM10 peptides to an excess of detergent (usually 4 mM).

Figure 1 shows the fluorescence emission spectra of mTM4 and mTM10 under different conditions. For mTM4 in buffer (Fig. 1a) Trp fluorescence intensity was significantly lower than that of NATA in water (which provides a reference value for a Trp residue exposed to an aqueous medium). In addition, emission was blue-shifted ($\lambda_{max} = 328.5$ nm), consistent with the formation of oligomers, as suggested by the kinetic data (online Fig. I). In contrast, fluorescence increased strongly after addition of mTM4 to preformed detergent micelles (fluorescence in DPC up to 2.4 times that of NATA in water) and a blue shift was observed, to 318.5 nm in DDM and 320 nm in DPC. We previously generated calibration curves for Trp λ_{max} as a function of Trp depth in DDM and DPC micelles, with a set of model polyLeu peptides containing a single Trp residue in different positions (de Foresta et al. 2002; Vincent et al. 2007). Comparison of the data presented here with these curves suggested that W142 in mTM4 (in position 11 relative to the N-terminus of the peptide) was embedded in the core of the peptide-detergent complex, with λ_{max} values intermediate between those of the P9 and P11 model peptides (Table 2 in Vincent et al. 2007). This provides a first indication that mTM4 spans the peptide-detergent complexes rather than remaining at their surface as described for TM16 and TM17.

The fluorescence intensity of mTM10 is also low in buffer, with λ_{max} at 329.5 nm (Fig. 1b). It increases in the presence of detergent micelles, but to a much lesser extent than that of mTM4. The maximum emission wavelengths also show a smaller blue shift, with the values obtained (327 and 331 nm in DDM and DPC, respectively) within the range of those observed for the P3, P5, and P7 model peptides (de Foresta et al. 2002; Vincent et al. 2007). This provided the first evidence that the position of W553 in mTM10 (in position 8 relative to the N-terminus of the peptide) was closer to the surface of the micelle than that of W142 in mTM4.

The fluorescence emission spectra of mTM4 and mTM10 were also recorded in TFE and in TFE/water (50:50, *v*/*v*), in which the helix-promoting effects of TFE may already be maximum (online Fig. II, A and B). Under

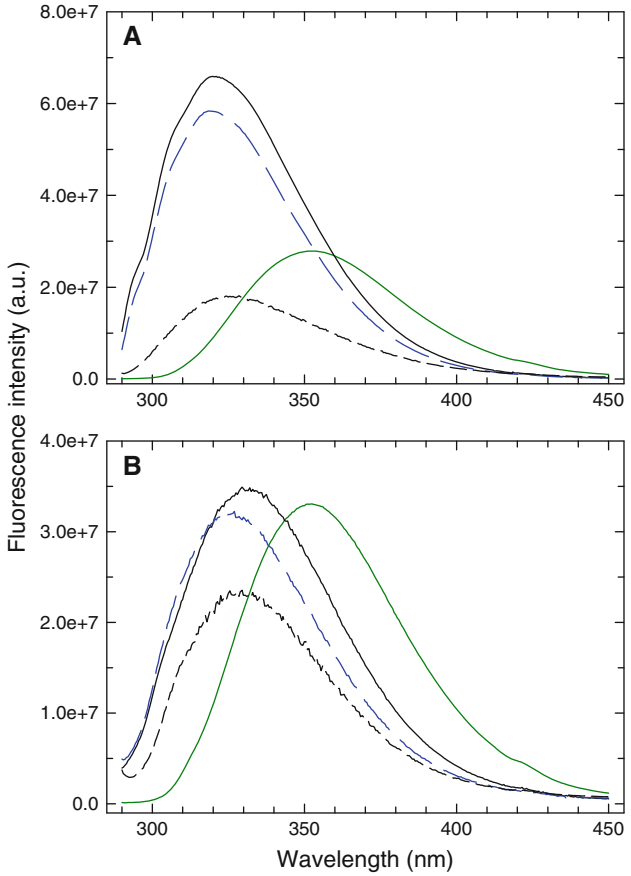

Fig. 1 Fluorescence emission spectra of the hMRP1 fragments in different media. **a** Emission spectra for 10 μM mTM4 in 10 mM phosphate buffer, pH 7.5, alone (*short dashed line*) or supplemented with 4 mM DPC (*continuous line*) or DDM (*blue long-dashed line*), at 20°C. λ_{ex} was set at 280 nm. Slit widths were 1.25 mm (bandwidths ~5 nm) for both excitation and emission. Spectra were recorded after a short period of equilibration (2–3 min) and the readings for background spectra (same solvent or detergent in buffer) were subtracted. **b** Emission spectra for 10 μM mTM10. *Same symbols* as in panel **a**. In both panels, the emission spectrum of 10 μM NATA in pure water is indicated as a reference (*green line*)

these conditions, Trp fluorescence was strongly quenched by TFE, as described elsewhere (Chen et al. 1995). The maximum emission wavelength (λ_{max}) of mTM4 in TFE is 340 nm, consistent with exposure of the Trp residue to this solvent (dielectric constant $\varepsilon = 26$ at 25°C). For mTM10, in addition to Trp fluorescence, Tyr (Y568) fluorescence was also visible, as a shoulder in the spectra at 307 nm.

Trp fluorescence quenching by acrylamide in mTM4 and mTM10 fragments incorporated into DDM and DPC micelles

We further evaluated Trp insertion into detergent micelles by assessing the accessibility of this residue to the neutral water-soluble fluorescence quencher acrylamide (Eftink 1991). The Stern–Volmer fluorescence quenching plots obtained for the mTM4 and mTM10 fragments in the presence of DDM or DPC micelles are shown in Fig. 2, panels a and b, respectively. Linear regressions were appropriate and typical of a collisional (dynamic) mechanism. The apparent accessibility to acrylamide of the Trp residues in mTM4 and mTM10 incorporated into detergent micelles was significantly lower than that of NATA in buffer, taken as a reference (Fig. 2a, b and K_{sv} in Table 2). In addition, for each fragment, Trp appeared less accessible to acrylamide in the presence of DDM than in the presence of DPC micelles. Comparisons of accessibility based on bimolecular quenching constants k_q are more accurate than those based on K_{sv}, because differences in the mean excited state lifetime of the Trp residue in the absence of quencher are taken into account ($k_q = K_{sv}/\langle\tau\rangle_i$, where $\langle\tau\rangle_i$ is the intensity-averaged lifetime) (Table 2). k_q values showed that the Trp residue of mTM4 was significantly shielded from the solvent (relative accessibility of 13 and 23% with NATA as reference, in DDM and DPC, respectively). By contrast, the Trp residue of mTM10 was more accessible to acrylamide than that of mTM4, in both detergents. These results are consistent with the finding that the Trp residues of both peptides were less accessible to aqueous solvent in DDM micelles than in DPC micelles.

Quenching by brominated detergents of the fluorescence of mTM4 and mTM10 fragments incorporated into DDM micelles

We investigated the location of the Trp residues of the TMs in the DDM micelles in more detail, by carrying out Trp quenching experiments with two brominated analogs of DDM: BrDDM, brominated at the C7 and C8 positions of the alkyl chain, and BrUM, brominated at the C10 and C11 positions, as previously described (de Foresta et al. 2010; Vincent et al. 2007). The two bromine atoms on the alkyl chain act as high-efficiency short-range quenchers. They enable detection of Trp–alkyl chain contacts.

We first recorded the fluorescence emission spectra of both fragments incorporated into DDM/BrDDM and DDM/BrUM mixed micelles containing different molar fractions of brominated detergent, ranging from 0 (pure DDM micelles in buffer) to 1 (pure BrDDM and BrUM micelles in buffer) (see online Fig. III, for mTM4). With both BrDDM (panel A) and BrUM (panel B) as quenchers, fluorescence intensity gradually decreased with increasing brominated detergent molar fraction, until almost complete quenching was achieved in pure brominated detergent micelles. The shape of the fluorescence spectra did not vary significantly with brominated detergent molar fraction, suggesting homogeneous location of the quenched Trp. Similar results were obtained with mTM10, but with

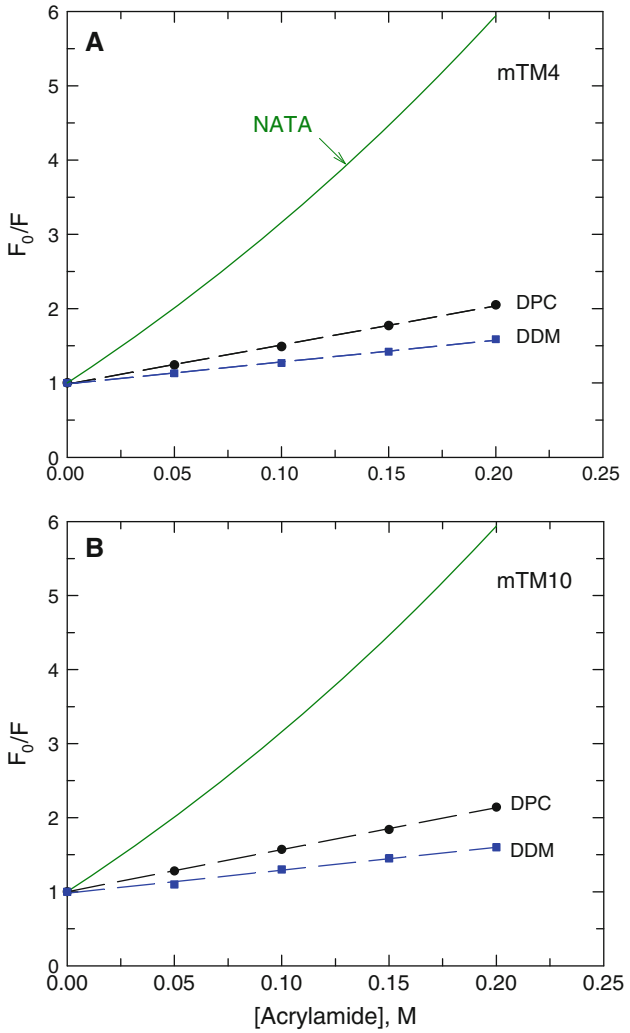

Fig. 2 Stern–Volmer plots of the quenching, by acrylamide, of the fluorescence of hMRP1 fragments in DPC and DDM micelles. **a** We added 5 μM mTM4 to 10 mM potassium phosphate buffer pH 7.5 supplemented with 4 mM DPC (*circles*) or DDM (*blue squares*), at 20°C. Aliquots of acrylamide were then added sequentially, at constant intervals (100 s). Fluorescence intensity was recorded continuously, with λ_{ex} set at 295 nm and λ_{em} set at 320 nm. Slit widths were 1.25 mm for excitation and 2.5 mm for emission. The fluorescence intensities obtained at each acrylamide concentration were corrected for blank values. The Stern–Volmer plot for NATA (5 μM) in buffer ($\lambda_{em} = 354$ nm in this case) is also shown, as a reference (*continuous green line*). A straight line was fitted to the data for MRP1 fragments, whereas the modified Stern–Volmer equation was used for NATA. **b** Similar experiment to those in panel **a**, but with 5 μM mTM10. λ_{em} was set at 340 nm in this case

significantly lower levels of fluorescence quenching (not shown).

We generated fluorescence quenching curves for mTM4 and mTM10 by plotting the fluorescence intensity at λ_{max} as a function of the molar fraction of BrDDM (Fig. 3a) or BrUM (Fig. 3b). Visual observation of the raw data suggests that the fluorescence of W142 in mTM4 is more sensitive to quenching by both brominated detergents than that of W553 in mTM10. A curve was fitted to the data, as described in "Materials and methods". The two parameters of the fit, n, the lattice parameter, related to the curvature, and F_{min}/F_0, the residual fluorescence in pure brominated detergent (i.e. at $X = 1$) are given in Table 3. In both detergents, the fluorescence of mTM4 was quenched more efficiently than that of mTM10, resulting in higher n values (e.g. with BrDDM, $n = 4.90$ and 3.48 for mTM4 and mTM10, respectively) and lower F_{min}/F_0 values (Table 3). Consistent with the differences in λ_{max} values (~8 nm blue shift of mTM4 relative to mTM10 in DDM; online Table I) and relative accessibility to acrylamide (13 and 20% for mTM4 and mTM10, respectively, in DDM; Table 2), these results strongly suggest that the W142 residue of mTM4 is located in the hydrophobic core of the micelles, whereas the W553 residue of mTM10 is in a more polar region. Moreover, a significant fraction of W553 (~20% according to F_{min}/F_0) is not in contact with the brominated chains of the detergent, even in pure BrDDM or BrUM. The insets in Fig. 3 provide a comparison of n values with the calibration data obtained with the set of PolyLeu model peptides (de Foresta et al. 2002; Vincent et al. 2007). In BrUM (Fig. 3b), the n value for mTM4 corresponds to that obtained for the model peptide P11 whereas n for mTM10 is lower than that for any of the model peptides, consistent with the conclusion drawn above. Surprisingly, in BrDDM, the n value for mTM4 was higher than those obtained for the model peptides. This may be because of the various approximations made in the model (including, in particular, the differences in lifetime between the various peptides not being taken into account) and/or differences in local conformations.

Time-resolved fluorescence intensity measurements for mTM4 and mTM10 in detergent micelles

MEM analyses of fluorescence intensity decays for both peptides in detergent provided the classic pattern of three excited-state lifetime populations with similar barycenter values (Fig. 4; Table 4). The major differences between the two peptides were the relative amplitudes of these populations. The excited-state lifetime distributions of W142 in mTM4 were dominated by the longest lifetime, $\tau_3 \sim 4$ ns (relative amplitude α_3 of ~70%) in DPC or DDM. The lifetime populations of W553 in mTM10 were more equally distributed, resulting in a significantly lower mean lifetime in each detergent, consistent with the lower steady-state fluorescence intensity of mTM10 than of mTM4. These differences between mTM4 and mTM10 probably result from differences in the type of secondary structure adopted by the segment bearing the Trp residue (Willis et al. 1994; and see "Discussion", below). For each fragment, the distributions differed only slightly between DPC and DDM.

Table 2 Results from the quenching, by acrylamide, of the fluorescence of mTM4 and mTM10 in DPC and DDM micelles

Sample	Medium	$\langle\tau\rangle_i$ (ns)	K_{sv} (M^{-1})	k_q (M^{-1} s^{-1}) (% of reference)
NATA	Buffer	3.0	17.5	5.83×10^9 (100%)
mTM4	DPC micelles	3.92	5.26	1.34×10^9 (23%)
mTM4	DDM micelles	3.75	2.94	0.78×10^9 (13%)
mTM10	DPC micelles	3.11	5.68	1.83×10^9 (31%)
mTM10	DDM micelles	2.65	3.1	1.17×10^9 (20%)

For peptides, the intensity-averaged lifetime values $\langle\tau\rangle_i$ were taken from Table 4. For NATA, $\langle\tau\rangle$ was taken from a previous study (Rouvière et al. 1997)

K_{sv} is the slope from Fig. 2. $k_q = K_{sv}/\langle\tau\rangle_i$

Time-resolved fluorescence anisotropy measurements for mTM4 and mTM10 in detergent micelles

The time-resolved fluorescence anisotropy of W142 in mTM4 incorporated into DPC or DDM micelles followed a double-exponential pattern of decay, with a ~1 ns time component (θ_1) probably reflecting local indole rotation and a time component one order of magnitude larger, θ_2 (Table 5). The values obtained for this time component were consistent with the Brownian rotational correlation time of the DPC and DDM micelles calculated with a spherical model (7.4 and 21 ns, respectively; Coïc et al. 2005). Thus, mTM4 was probably incorporated as a monomer into both types of detergent micelle. The amplitude of the internal motion of the indole ring, estimated from the semi-angle of the wobbling-in-cone model (Kinosita et al. 1977), was slightly smaller in DDM than in DPC micelles.

For W553 in mTM10, anisotropy showed an additional infinite time component (θ_3) in DPC, indicating probable partial association of mTM10 in these detergent micelles, as previously reported for mTM16 (de Foresta et al. 2010). In DDM, the longest rotational correlation time was in the same range as that for pure micelles (Table 5). The initial anisotropy values $A_{t=0}$ for mTM4 in both DPC and DDM and for mTM10 in DPC were similar to the intrinsic anisotropy of NATA in vitrified medium at the same excitation wavelength (290 nm) (Rouvière et al. 1997), indicating the absence of rotational motion occurring over less than ~0.7–0.9 ns in these experiments. For mTM10, subnanosecond rotation probably occurred in DDM, because the $A_{t=0}$ value was lower than the intrinsic anisotropy of NATA.

Far-UV circular dichroism (CD) study of mTM4 and mTM10 in different media

We investigated the secondary structure of mTM4 and mTM10 in different media, by conducting a far-UV CD study. The CD spectrum of mTM4 in pure TFE is indicative of a predominantly α-helical conformation, with a characteristically high maximum at ~192 nm and two minima at 208 and 220 nm (Fig. 5a). Deconvolution of this spectrum indicated the presence of 72% α-helix, with minor contributions of other non-helical structures (β-strands, turns, and unordered). This folding of mTM4 into α-helix was already achieved at 50% (*v*/*v*) TFE in buffer (not shown). Unlike the hMRP1 TM16 and TM17 fragments previously studied, mTM4 conserved its α-helical folding when this fragment was incorporated into DPC and DDM micelles (with α-helix contents of ~70 and 60%, respectively).

mTM10 also adopted a principally α-helical structure in pure TFE (55% α-helix according to the deconvolution; Fig. 5b), but this was significantly less marked than for mTM4. Furthermore, this structure was not fully achieved in 50% TFE (40% α-helix content, not shown). In the presence of DPC or DDM micelles, the α-helix content of mTM10 fell below 20 and 10%, respectively, with a corresponding increase in the contribution of non-helical structures.

We then compared the structure of mTM4 in the presence of pure DDM, BrDDM, and BrUM micelles in buffer (Fig. 6). As in DDM, this fragment was also mostly α-helical in pure brominated detergent micelles, and its helical content was even slightly greater (up to 67% in BrDDM). These results demonstrate that the brominated detergents used as fluorescence quenchers in mixed micelles do not themselves induce significant changes in peptide structure.

Discussion

Most membrane proteins are poorly abundant in their native environment. Unlike functional studies, structural studies of these proteins require significant amounts of highly purified protein. These proteins are therefore generally produced in various heterologous systems (*E. coli*, yeast, insect cells etc.), and purified, with appropriate

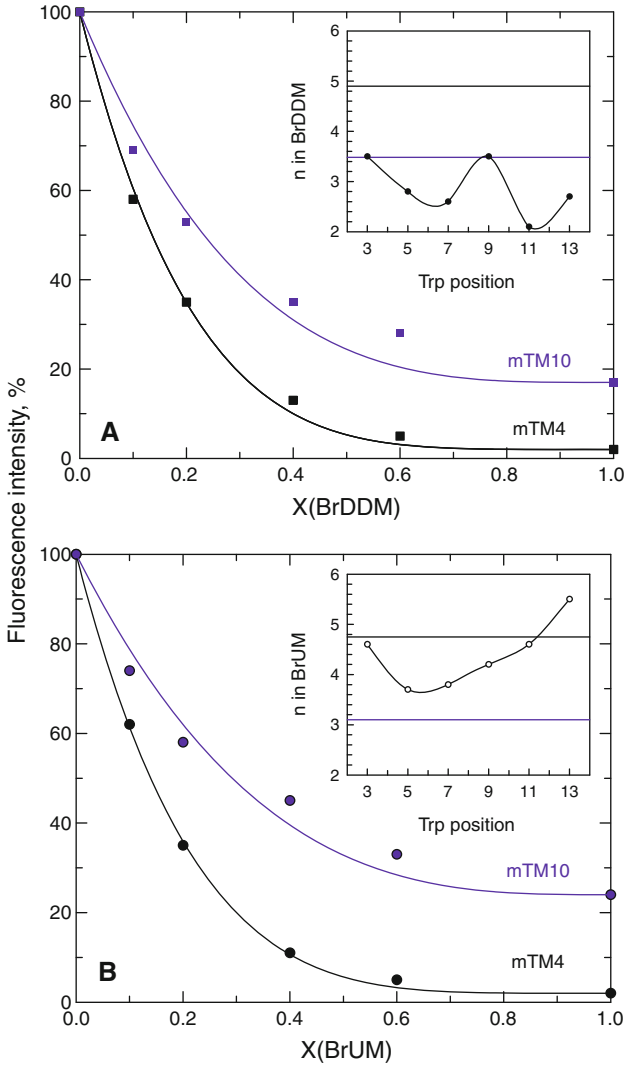

Fig. 3 Quenching of the fluorescence of hMRP1 fragments in mixed micelles of BrDDM/DDM (**a**) or BrUM/DDM (**b**). **a** The maximum fluorescence intensity of the spectra for mTM4 at $\lambda_{em} = 318.5$ nm (*black symbols*) (from online Fig. III) and mTM10 at $\lambda_{em} = 327.5$ nm (*violet symbols*) is plotted as a function of the molar fraction (X) of BrDDM. A curve was fitted to the data, as described in "Materials and methods". The *inset* show the calibration curves of n against Trp position, for six model peptides in BrDDM/DDM (de Foresta et al. 2002). The *horizontal lines* represent the n values obtained here for the hMRP1 fragments. **b** Similar experiment to that in panel **a**, but with BrUM as the brominated detergent

Table 3 Fluorescence quenching curve data for mTM4 and mTM10 in mixed micelles of DDM with BrDDM or BrUM

Fragment	Mixed micelles	n	F_{min}/F_0 (%)
mTM4	DDM/BrDDM	4.90	2
mTM4	DDM/BrUM	4.75	2
mTM10	DDM/BrDDM	3.48	17
mTM10	DDM/BrUM	3.10	24

n and F_{min}/F_0 were obtained from the fit of the quenching curves in Fig. 3

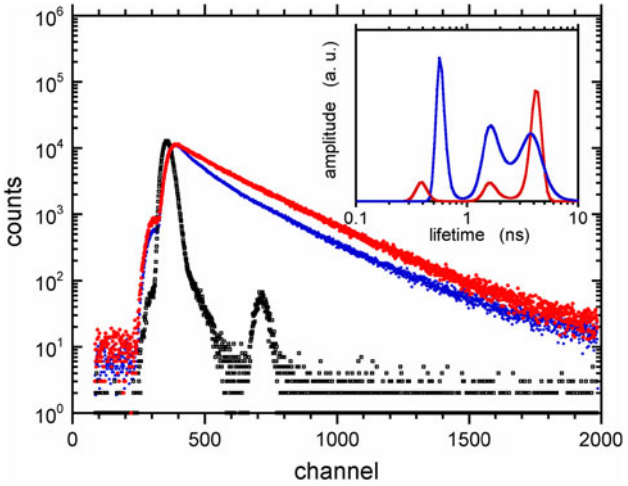

Fig. 4 Time-resolved fluorescence of hMRP1 fragments in DPC micelles. Fluorescence intensity decays of mTM4 (*red trace*) and mTM10 (*blue trace*) in DPC. Instrumental response function (*black trace*). *Inset* excited-state lifetime distribution obtained from MEM analysis for mTM4 (*red trace*) and mTM10 (*blue trace*) in DPC

detergents. This procedure has proved successful for some proteins, but the isolation of others remains difficult. Thus, although ~5,500 human genes are thought to code for membrane proteins identified by seven topology prediction methods (Fagerberg et al. 2010), high-resolution structures are currently only available for 14 such proteins from humans. For all the species studied, only ~250 such structures are available (http://blanco.biomol.uci.edu/Membrane_Proteins_xtal.html#Latest). An alternative method for studying the structural properties of membrane proteins is to study isolated parts of these proteins, for example transmembrane fragments incorporated into membrane-mimic systems, for example detergent micelles or liposomes. This "divide and conquer" approach surmises that the isolated predicted TM peptides behave in these membrane mimics as in the full-length parent protein. Important results obtained with this approach have recently been extensively reviewed (Bordag and Keller 2010). Our understanding of the membrane interactions of TM fragments has recently been improved by studies of their native insertion mechanism, which involves a membrane complex, the Sec61 translocon (White and von Heijne 2005). However, whatever the folding pathway, membrane proteins are expected to be at a free energy minimum, at least a local one. Global minima have been directly demonstrated in a few membrane protein refolding experiments only (Di Bartolo et al. 2011; Stanley and Fleming 2008 and references cited therein).

hMRP1 is a high-molecular-weight membrane protein with 17 predicted TM fragments. Such large membrane proteins are relatively scarce, because only 5% of membrane proteins are predicted to have more than 12 TMs,

Table 4 Fluorescence intensity decay data for the Trp residue in mTM4 and mTM10 in DPC and DDM micelles

Peptide	Detergent micelles	α_1	α_2	α_3	τ_1 (ns)	τ_2 (ns)	τ_3 (ns)	$\langle\tau\rangle_i$ (ns)[a]
mTM4	DPC	0.12 ± 0.02	0.20 ± 0.04	0.68 ± 0.04	0.43 ± 0.05	1.93 ± 0.24	4.25 ± 0.12	3.92 ± 0.07
mTM4	DDM	0.14 ± 0.01	0.15 ± 0.05	0.71 ± 0.05	0.54 ± 0.03	1.69 ± 0.04	4.01 ± 0.20	3.75 ± 0.04
mTM10	DPC	0.32 ± 0.03	0.40 ± 0.06	0.28 ± 0.08	0.58 ± 0.01	1.91 ± 0.18	4.28 ± 0.37	3.11 ± 0.01
mTM10	DDM	0.34 ± 0.01	0.36 ± 0.02	0.30 ± 0.01	0.53 ± 0.07	1.63 ± 0.04	3.57 ± 0.04	2.65 ± 0.03

Mean values ± standard errors for two measurements are given

[a] $\langle\tau\rangle_i$, the intensity-averaged lifetime was calculated as $\langle\tau\rangle_i = \Sigma\alpha_i\tau_i^2/\Sigma\alpha_i\tau_i$

Table 5 Fluorescence anisotropy decay data for the Trp residue in mTM4 and mTM10 in DPC and DDM micelles

Peptide	Detergent micelles	β_1	β_2	β_3	θ_1 (ns)	θ_2 (ns)	θ_3 (ns)	ω_{max} (°)	$A_{t=0}$
mTM4	DPC	0.040 ± 0.002	0.094 ± 0.004	–	0.9 ± 0.1	8.5 ± 0.2	–	27 ± 2	0.134 ± 0.006
mTM4	DDM	0.023 ± 0.003	0.112 ± 0.001	–	0.7 ± 0.2	15.1 ± 0.6	–	20 ± 1	0.135 ± 0.004
mTM10	DPC	0.054 ± 0.001	0.058 ± 0.003	0.036 ± 0.007	0.4 ± 0.1	5.9 ± 0.5	∞	27 ± 4	0.148 ± 0.011
mTM10	DDM	–	0.024 ± 0.008	0.084 ± 0.001	–	1.6 ± 0.2	26 ± 1	22 ± 4	0.108 ± 0.009

The anisotropy β_i is the area and the rotational correlation time θ_i is the barycenter of peak i for the rotational correlation time distribution. $A_{t=0}$ is the anisotropy at time zero, with $A_{t=0} = \Sigma\beta_i$. The semi-angle ω_{max} of the wobbling-in-cone subnanosecond motion was calculated from: $\Sigma\beta_{ns}/A_0 = [1/2\cos\omega_{max}(1 + \cos\omega_{max})]^2$, which gives: $\omega_{max} = \text{Arccos}1/2[(1 + 8(\Sigma\beta_{ns}/A_0)^{1/2})^{1/2} - 1]$, where A_0 is Trp anisotropy in the absence of depolarization and β_{ns} is the anisotropy of the nanosecond components. The A_0 value at an excitation wavelength of 290 nm was 0.134, as measured for NATA in vitrified medium (Rouvière et al. 1997). Mean values ± standard errors for two measurements are given

with some having up to 33 TMs (Fagerberg et al. 2010). Partial insight into the structure of hMRP1 (MSD1 and MSD2, containing 12 TMs) was initially obtained by homology modeling based on the crystal structure of the bacterial ABC transporter Sav 1866 from *Staphylococcus aureus* (DeGorter et al. 2008). A 3D structure was recently proposed for hMRP1 on the basis of electron cryomicroscopy data for 2D crystals (Rosenberg et al. 2010) and the core structure was compared with the structure of murine PgP (Aller et al. 2009). Various reviews have dealt with the transport mechanism, which may have general characteristics common to other ABC transporters (Jones et al. 2009; Locher 2009; Rees et al. 2009) but also has specific characteristics, because of GSH cotransport, in particular (Borst et al. 2006; Chang 2010; Cole and Deeley 2006; Deeley and Cole 2006; Deeley et al. 2006). The general transport cycle may be analyzed structurally with data for the bacterial ABC lipid flippase MsbA, for which four X-ray structures have been generated: two apo-bound and two nucleotide-bound states (Ward et al. 2007). In the absence of nucleotide, one structure (open apo) has a V shape, with the opening facing the intracellular medium, for the binding of intracellular substrates. A more closed structure is also obtained (closed apo). ATP binding triggers a conformational change resulting in the opening of the binding pocket toward the extracellular medium (outward facing conformation) (Kerr et al. 2010; Ward et al. 2007).

We recently began a study of hMRP1 predicted TM fragments, focusing initially on TM16 and TM17, which have been implicated in transport in various functional studies. The work described here highlights striking differences in the membrane insertion features, in membrane mimics composed of detergent micelles, of two predicted TM fragments, TM4 and TM10, from MSD0 and MSD, respectively. The function of MSD0 remains unclear, whereas MSD1 is probably involved in transmembrane substrate transport.

We chemically synthesized two 25-amino acid peptides with sequences similar to those of the predicted native fragments (Table 1). Both TMs are hydrophobic, as shown by their interfacial partitioning free energy for unfolded peptide (ΔG_u), which was −5.4 kcal/mol for mTM4 and −7.4 kcal/mol for mTM10 (Table 1). For all predicted TMs, ΔG_u values ranged from −0.82 (for TM9) to −14.7 kcal/mol (for TM1) (online Table II). We obtained stable peptide–detergent complexes by solubilizing the TMs in the α-helix-promoting solvent TFE and then diluting them in an aqueous micellar solution of DPC, a zwitterionic detergent, or DDM, a neutral one. Our experience of such peptides has led us to favor the use of detergents (and these two in particular) as membrane mimics (de Foresta et al. 2010; Vincent et al. 2007), along with other authors (Bordag and Keller 2010). The assessment of mTM4 insertion into micelles of both detergents

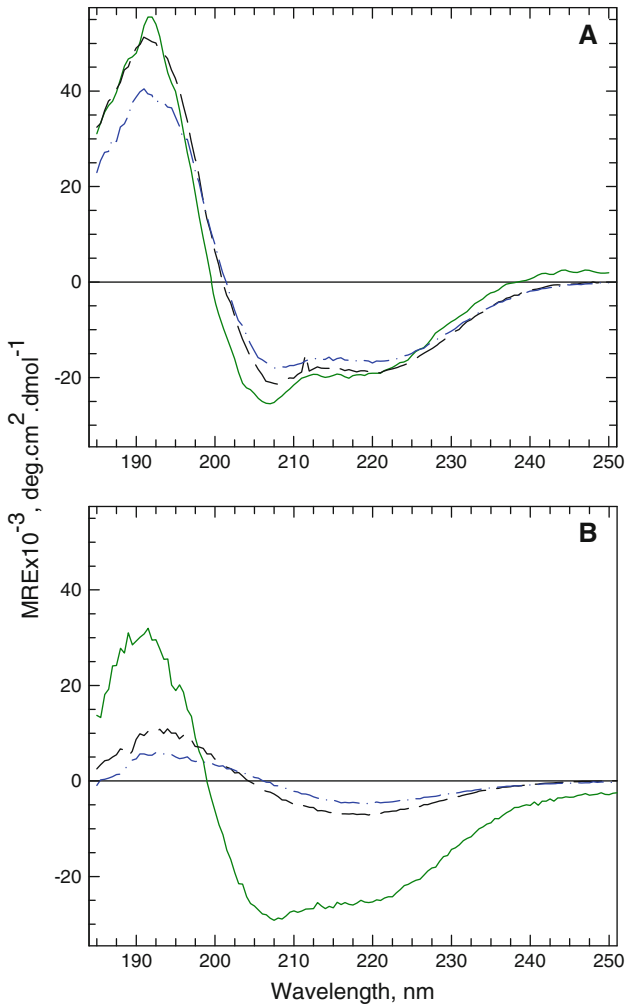

Fig. 5 Far-UV CD spectra for mTM4 and mTM10 in various media. **a** CD spectra for mTM4, normalized in mean residue ellipticity. The medium was TFE (*green continuous line*), or buffer containing 4 mM DPC (*black long-dashed line*) or DDM (*blue dashed–dotted line*). $T = 20$°C. **b** CD spectra for mTM10. *Same symbols* as in panel **a**

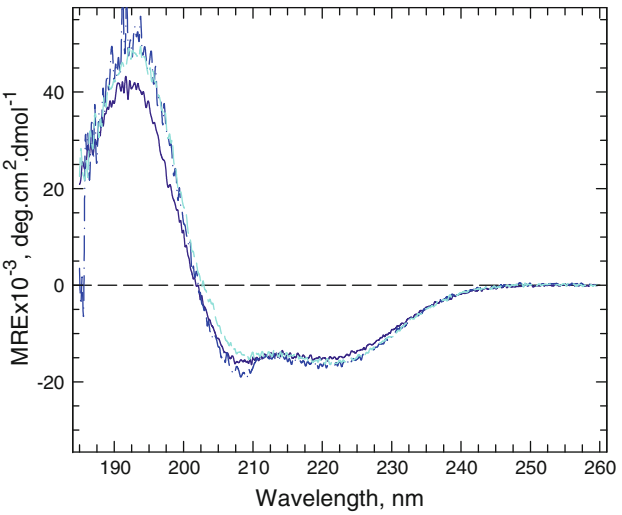

Fig. 6 Far-UV CD spectra for mTM4 in DDM, BrDDM, and BrUM micelles. CD spectra for mTM4. The medium was buffer containing 2 mM DDM (*dark blue continuous line*), BrDDM (*blue dashed-dotted line*), or BrUM (*cyan dotted line*). $T = 20$°C. These experiments were performed with 0.2 nm wavelength increments, an integration time of 1 s, and five scans

was sensitive, as demonstrated by the ~30 nm blue shift in Trp fluorescence λ_{max} and in the doubling of fluorescence intensity relative to NATA in aqueous buffer, which was used as a soluble, uncharged Trp model. For mTM10, a ~20 nm blue shift for λ_{max} was observed, with respect to NATA, with no significant change in fluorescence intensity. Furthermore, the interaction of mTM4 and mTM10 with DDM micelles was also clearly demonstrated by the almost 100 and 80% fluorescence quenching observed in the brominated detergent micelles, indicating almost permanent contact between the Trp residues of these TMs and detergent acyl chains.

For mTM4, the peptide-detergent micelles were similar in size to the corresponding pure detergent micelles, given the longer rotational correlation time values obtained in time-resolved fluorescence anisotropy measurements. For mTM10, complexes larger in size than the pure micelles may have been formed.

Four principal properties were used to characterize the depth of Trp insertion within the peptide-detergent complexes: λ_{max}, which is sensitive to polarity and rate of relaxation of polar groups in the Trp microenvironment; k_q, which characterizes Trp accessibility to acrylamide, measured in the presence of DPC or DDM micelles; n, and F_{min}/F_0, which characterize Trp accessibility to brominated acyl chains in the presence of DDM/BrDDM and DDM/BrUM mixed micelles. The results obtained for all four were consistent with deeper insertion of the Trp residue of mTM4 than of that of mTM10 in the peptide–detergent assemblies. Indeed, a smaller λ_{max} was observed for mTM4 than for mTM10, corresponding to an environment of lower polarity, together with a lower k_q corresponding to lower accessibility to the water-soluble acrylamide in the presence of DPC or DDM. We also obtained greater n values for mTM4 than for mTM10, n reflecting the number of brominated groups that may be simultaneously (or within a very short time interval) in contact with Trp, and lower F_{min}/F_0 values indicating stronger quenching in pure brominated detergent micelles (BrDDM or BrUM). The Trp residue of each peptide was accessible to at least one of the two quenchers, as the two quenching processes resulted in the quenching of almost 100% of the observed fluorescence (as seen from the relative accessibility to acrylamide in Table 2 and that to brominated detergent, "$100 - F_{min}/F_0$", from Table 3).

These values were compared with those of appropriate calibration data, obtained with α-helical transmembrane model peptides bearing a Trp residue at different positions in the sequence, in DDM (de Foresta et al. 2002) and in DPC micelles (Vincent et al. 2007). For mTM4, most of the values obtained were most similar to those for P9 and/or P11, whereas, for mTM10, they were more similar to those for P3, P5, or P7. However, some of the values were out of the calibration range: for instance, *n* for mTM10 (3.1) was smaller than any of the *n* values for the model peptides (range 3.7–5.6). Similar behavior has previously been observed with other biological peptides studied in the same micellar systems (for example fragment 94–102 of caveolin-1, and mTM16 and mTM17; de Foresta et al. 2010; Le Lan et al. 2010; Vincent et al. 2007). There are several possible reasons for this, including partial self-association of the peptides on the micellar surface (mTM16 and mTM17), heterogeneity in the location of the Trp residue (caveolin fragment), and/or differences in the local conformation of the Trp residue, as inferred from a comparison of excited-state lifetime distributions with those for model transmembrane Pn peptides.

We first studied the secondary structure of these predicted TMs in TFE, to determine experimentally their tendency to fold into an α-helix. TFE has long been known to reveal the tendency of otherwise unfolded peptides to form helices (Jasanoff and Fersht 1994) or β-sheet structures (Reiersen and Rees 2000). The structures adopted by various peptides as a function of TFE–water mole fraction often have a sharp transition at a concentration well below pure TFE, often at ∼20% TFE (*v*/*v*), with a maximum at 40–50% TFE, but these values may vary with the propensity of the peptide to form helices (Bouhss et al. 1996; Buck 1998; Jasanoff and Fersht 1994; Lequin et al. 2006; Montserret et al. 1999). The basis of this effect has long been a matter of debate and various mechanisms have been suggested (Buck 1998). Consistent with previous proposals, molecular dynamics simulations of peptides for a duration of 20 ns in TFE–water mixtures indicated that TFE molecules aggregated around the peptides, thereby removing the hydrogen-bonding partner and providing a weakly dielectric environment favoring intrapeptide hydrogen bonding (Roccatano et al. 2002).

In pure TFE, mTM4 was predominantly folded as an α-helix (>70%), to a substantially greater extent than was mTM10 (55%). The different tendency of the two TMs to form helices was further exemplified by the higher TFE concentration required for the random coil to α-helix transition for mTM10 than for mTM4.

The tendency of amino acids to form helices differs between different membrane environments and in buffer, and was quantified for uncharged amino acids with a set of designed model peptides solubilized in SDS micelles (Li and Deber 1994). Comparisons of TM amino acid content on this scale showed that mTM4 contained more α-helix-promoting amino acids (with two Ile, three Val, and five Leu residues, with the strongest helical propensity) than mTM10 (with five Thr residues with a lower helical propensity), consistent with our experimental data.

The folding differences between mTM4 and mTM10 were even more marked in the presence of DPC or DDM micelles. The major structural component of mTM4 continued to be α-helix in both detergents (∼60% on average), whereas the α-helix became a minor component for mTM10 in detergent (10%, on average). Our findings for mTM4 suggest that 15 of the 25 residues adopted an α-helical conformation, corresponding to at least four helix turns.

These differences in folding between the two peptides affected the local conformation of the Trp residue, as shown by excited-state lifetime measurements. The multiexponential pattern of Trp fluorescence intensity decay, with three lifetime populations, as observed for W142 in mTM4 and W553 in mTM10, is also frequently observed for many peptides or proteins containing a single Trp residue (Lakowicz 2006). This multiexponential nature of Trp fluorescence intensity decay can sometimes be explained by dipolar relaxation of the environment, as demonstrated for indole (Vincent et al. 1995) and shown for some proteins (Vincent et al. 2000). However, it is more generally interpreted in the context of the rotamer model (Szabo and Rayner 1980), in which a variety of structural constraints are imposed by the folding of the main peptide chain and specifically favor each of the Trp rotamer populations. The multiple fluorescence lifetimes are attributed to differences in the rate of excited-state electron transfer from Trp to peptide bonds between rotamers (Ababou and Bombarda 2001; Adams et al. 2002). A clear relationship has been established between the relative amplitude of the longest excited-state lifetime, characterizing the *t* rotamer, which has the smallest number of steric contacts with the peptide skeleton, and α-helix content (Bouhss et al. 1996; Willis et al. 1994). In the work presented here, the excited-state lifetime values of W142 in mTM4 and W553 in mTM10 were very similar and within the range characteristic of Cα-Cβ Trp χ_1 rotamers in conformationally constrained peptides (Pan and Barkley 2004), but very different amplitudes were obtained. The excited-state lifetime distribution of W142 in mTM4 was principally dominated, in both DDM and DPC micelles, by the long lifetime signature of the *t* rotamer, consistent with the principally α-helical structure of the peptide, as demonstrated by CD measurements. Conversely, the excited-state lifetime distribution of W553 in mTM10 was more heterogeneous, consistent with a predominance of non α-helical structures.

The principally α-helical folding of mTM4 may make a major contribution to the free energy of partition of this

peptide in micelles: if, as estimated by the MPEX site, each residue involved in an α-helix contributes approximately −0.4 kcal/mol to the ΔG of the folded peptide, the ΔG value is approximately −11.4 kcal/mol. Together with the fluorescence data locating W142 in the core of the micelle, these results strongly suggest that mTM4 is inserted radially into the micelle. A U-shape configuration of mTM4 would not be excluded by the fluorescence data but the lack of helix-breaker amino-acid in the center of the peptide makes this configuration less probable than the presence of a single straight helix crossing the micelle. The size of both DPC and DDM pure micelles, respectively spherical and ellipsoidal with at least one diameter of ∼40–50 Å (Dupuy et al. 1997; Lauterwein et al. 1979; see also Abel et al. 2010), enables such a configuration with polar and charged ends of the peptide being in contact with the solvent. This configuration would be expected for a predicted TM fragment, but this remains the only hMRP1 fragment shown to behave in this way. We previously showed that isolated TM16 and TM17 seemed to be interfacial and that TM16 seemed to self-associate at the micelle surface. Such an interfacial position was also supported by recent molecular dynamics simulation (50 ns long) of these peptides in DDM micelles (S. Abel et al., in preparation). These results also show that TM10 is probably confined to the polar region of the micelles, with its low α-helix content making only a minor contribution to its free energy of partition into the micelles.

In our experience, for amphiphilic peptides located at/close to the surface of the detergent micelles (hMRP1 TM10, TM16, and TM17 (de Foresta et al. 2010; Vincent et al. 2007) and a small caveolin1 fragment (Le Lan et al. 2010)), and for transmembrane peptides (TM4), CD spectra systematically indicate a slightly lower helical content in DDM than in DPC. Caution is required when interpreting small differences between CD spectra obtained in heterogeneous media, such as micelles or membranes (different local refraction indices), but these differences were often found to be correlated with a weaker solubilization effect of DDM observed by other methods (e.g. fluorescence). For our peptides, DPC is, therefore, probably the better detergent for revealing the tendency to form α-helix structures.

If TM10 does not spontaneously adopt a transverse position within the membrane, its insertion may be driven by TM–TM interactions. According to the resolved structures of other ABC transporters, the packing of TMs within the membrane suggests that individual TMs do not necessarily interact with their closest neighbors in the sequence. These structures are indicative of substantial twisting of the various helices and, based on the schematic V-shaped model, each side of the V is formed from TMs belonging to both the MSD1 and MSD2 domains. Furthermore, TM packing differs between the inward and outward conformations. For ABC homodimers, TMs 1–3 and 6 from one subunit (or MSD) interact with TMs 4–5 of the other subunit in the inward state, and TMs 1–2 from one subunit interact with TMs 3–6 from the other subunit in the outward state (Rees et al. 2009). For hMRP1, this corresponds, for the side containing TM10, to a packing of TMs 9–10 (from MSD1) with TMs 12–13–14 and 17 (MSD2) in the inward state, and of TMs 8–9–10–11 (MSD1) with TMs 12–13 (MSD2) in the outward conformation, as modeled in a previous study (DeGorter et al. 2008). In this outward conformation, TM10 may be spatially close to TMs 9, 11, 12, and 13 (DeGorter et al. 2008). TM10 is uncharged, so no ionic interactions would be predicted. TMs 9, 10, and 11 each contain a central proline residue that may facilitate the twisting of the helices.

By contrast, TM4 spontaneously inserts into the membrane as an α-helix. It may also interact with the TMs of the other domains, as a helix–helix interaction motif, AxxxA (ALVCA), has been identified in the C-terminal half of the peptide.

Conclusion

This report describes the behavior of two predicted transmembrane fragments of hMRP1, TM4 from MSD0 and TM10 from MSD1, in various media including detergent micelles and TFE. Taking into account our previous studies of TM16 and TM17 from MSD2 (de Foresta et al. 2010; Vincent et al. 2007), we are now able to compare fragment properties from the three membrane domains of this protein. We show here that TM4 seems to be structured as an α-helix and to span as a monomer the micellar complex it forms with DPC or DDM. By contrast, TM10 is located in the polar headgroup region of membrane mimics, as already described for TM16 and TM17. In this location, these three fragments are only partially folded into α-helix and tend to self-associate. These results add to our knowledge of membrane protein folding and provide new examples of marginally hydrophobic TMs which do not spontaneously insert in a transmembrane position. The insertion of such TMs into the membrane should be guided by local sequence context (loops and neighboring TMs) or interaction with more distant parts of the protein (Hedin et al. 2010 and references cited therein). Such TMs are more frequently found in ion channels and small molecule transporters (other ABC proteins, for example P-glycoprotein, the cystic fibrosis transmembrane conductance regulator, or EmrD; Hedin et al. 2010). For hMRP1, we notice that TM10, TM16, and TM17 contain amino-acid residues shown to take part in substrate translocation (Ito et al. 2001; Karwatsky et al. 2003; Situ et al. 2004; Zhang et al. 2002). As for TM4, its stable transverse insertion into

membrane mimics suggests that, in the context of the full-length hMRP1 transporter, this insertion does not require other protein loops and TMs. MSD0 as a whole, which contains the most hydrophobic hMRP1 TMs (online Table II) is likely to be more stable in the membrane than MSD1 and MSD2, both these domains requiring more flexibility because they are directly involved in the transport pathway.

References

Ababou A, Bombarda E (2001) On the involvement of electron transfer reactions in the fluorescence decay kinetics heterogeneity of proteins. Protein Sci 10:2102–2113

Abel S, Dupradeau FY, Raman EP, MacKerell AD Jr, Marchi M (2010) Molecular simulations of dodecyl-β-maltoside micelles in water: influence of the headgroup conformation and force field parameters. J Phys Chem B 115:487–499

Adams PD, Chen Y, Ma K, Zagorski MG, Sönnichsen FD, McLaughlin ML, Barkley MD (2002) Intramolecular quenching of tryptophan fluorescence by the peptide bond in cyclic hexapeptides. J Am Chem Soc 124:9278–9286

Aller SG, Yu J, Ward A, Weng Y, Chittaboina S, Zhuo R, Harrell PM, Trinh YT, Zhang Q, Urbatsch IL, Chang G (2009) Structure of P-glycoprotein reveals a molecular basis for poly-specific drug binding. Science 323:1718–1722

Ambudkar SV, Kimchi-Sarfaty C, Sauna ZE, Gottesman MM (2003) P-glycoprotein: from genomics to mechanism. Oncogene 22:7468–7485

Babenko AP, Bryan J (2003) Sur domains that associate with and gate KATP pores define a novel gatekeeper. J Biol Chem 278: 41577–41580

Bakos E, Evers R, Szakacs G, Tusnady GE, Welker E, Szabo K, de Haas M, van Deemter L, Borst P, Varadi A, Sarkadi B (1998) Functional multidrug resistance protein (MRP1) lacking the N-terminal transmembrane domain. J Biol Chem 273:32167–32175

Bernsel A, Viklund H, Falk J, Lindahl E, von Heijne G, Elofsson A (2008) Prediction of membrane-protein topology from first principles. Proc Natl Acad Sci USA 105:7177–7181

Bordag N, Keller S (2010) Alpha-helical transmembrane peptides: a "divide and conquer" approach to membrane proteins. Chem Phys Lipids 163:1–26

Borst P, Elferink RO (2002) Mammalian ABC transporters in health and disease. Annu Rev Biochem 71:537–592

Borst P, Zelcer N, van de Wetering K, Poolman B (2006) On the putative co-transport of drugs by multidrug resistance proteins. FEBS Lett 580:1085–1093

Bouhss A, Vincent M, Munier H, Gilles AM, Takahashi M, Bârzu O, Danchin A, Gallay J (1996) Conformational transitions within the calmodulin-binding site of *Bordetella pertussis* adenylate cyclase studied by time-resolved fluorescence of Trp242 and circular dichroism. Eur J Biochem 237:619–628

Bowie JU (2005) Solving the membrane protein folding problem. Nature 438:581–589

Buck M (1998) Trifluoroethanol and colleagues: cosolvents come of age. Recent studies with peptides and proteins. Q Rev Biophys 31:297–355

Chan KW, Zhang H, Logothetis DE (2003) N-terminal transmembrane domain of the SUR controls trafficking and gating of Kir6 channel subunits. EMBO J 22:3833–3843

Chang XB (2010) Molecular mechanism of ATP-dependent solute transport by multidrug resistance-associated protein 1. Methods Mol Biol 596:223–249

Chen Y, Liu B, Barkley MD (1995) Trifluoroethanol quenches indole fluorescence by excited-state proton-transfer. J Am Chem Soc 117:5608–5609

Chen Q, Yang Y, Li L, Zhang JT (2006) The amino terminus of the human multidrug resistance transporter ABCC1 has a U-shaped folding with a gating function. J Biol Chem 281:31152–31163

Chenal A, Guijarro JI, Raynal B, Delepierre M, Ladant D (2009) RTX calcium binding motifs are intrinsically disordered in the absence of calcium: implication for protein secretion. J Biol Chem 284:1781–1789

Coïc YM, Vincent M, Gallay J, Baleux F, Mousson F, Beswick V, Neumann JM, de Foresta B (2005) Single-spanning membrane protein insertion in membrane mimetic systems: role and localization of aromatic residues. Eur Biophys J 35:27–39

Cole SP, Deeley RG (2006) Transport of glutathione and glutathione conjugates by MRP1. Trends Pharmacol Sci 27:438–446

Cole SP, Bhardwaj G, Gerlach JH, Mackie JE, Grant CE, Almquist KC, Stewart AJ, Kurz EU, Duncan AM, Deeley RG (1992) Overexpression of a transporter gene in a multidrug-resistant human lung cancer cell line. Science 258:1650–1654

Dawson RJ, Locher KP (2006) Structure of a bacterial multidrug ABC transporter. Nature 443:180–185

Dawson RJ, Locher KP (2007) Structure of the multidrug ABC transporter Sav1866 from Staphylococcus aureus in complex with AMP-PNP. FEBS Lett 581:935–938

de Foresta B, Legros N, Plusquellec D, le Maire M, Champeil P (1996) Brominated detergents as tools to study protein-detergent interactions. Eur J Biochem 241:343–354

de Foresta B, Gallay J, Sopkova J, Champeil P, Vincent M (1999) Tryptophan octyl ester in detergent micelles of dodecylmaltoside: fluorescence properties and quenching by brominated detergent analogs. Biophys J 77:3071–3084

de Foresta B, Tortech L, Vincent M, Gallay J (2002) Location and dynamics of tryptophan in transmembrane alpha-helix peptides: a fluorescence and circular dichroism study. Eur Biophys J 31:185–197

de Foresta B, Vincent M, Gallay J, Garrigos M (2010) Interaction with membrane mimics of transmembrane fragments 16 and 17 from the human multidrug resistance ABC transporter 1 (hMRP1/ABCC1) and two of their tryptophan variants. Biochim Biophys Acta 1798:401–414

Dean M, Allikmets R (2001) Complete characterization of the human ABC gene family. J Bioenerg Biomembr 33:475–479

Deeley RG, Cole SP (2006) Substrate recognition and transport by multidrug resistance protein 1 (ABCC1). FEBS Lett 580: 1103–1111

Deeley RG, Westlake C, Cole SP (2006) Transmembrane transport of endo- and xenobiotics by mammalian ATP-binding cassette multidrug resistance proteins. Physiol Rev 86:849–899

DeGorter MK, Conseil G, Deeley RG, Campbell RL, Cole SP (2008) Molecular modeling of the human multidrug resistance protein 1 (MRP1/ABCC1). Biochem Biophys Res Commun 365:29–34

Di Bartolo ND, Hvorup RN, Locher KP, Booth PJ (2011) In Vitro folding and assembly of the *Escherichia coli* ATP-binding cassette transporter, BtuCD. J Biol Chem 286:18807–18815

Dupuy C, Auvray X, Petipas C, Rico-Lattes I, Lattes A (1997) Anomeric effects on the structure of micelles of alkyl maltosides in water. Langmuir 13:3965–3967

East JM, Lee AG (1982) Lipid selectivity of the calcium and magnesium ion dependent adenosinetriphosphatase, studied with fluorescence quenching by a brominated phospholipid. Biochemistry 21:4144–4151

Eftink MR (1991) Fluorescence techniques for studying protein structure. Methods Biochem Anal 35:127–205

Engelman DM, Chen Y, Chin CN, Curran AR, Dixon AM, Dupuy AD, Lee AS, Lehnert U, Matthews EE, Reshetnyak YK, Senes

A, Popot JL (2003) Membrane protein folding: beyond the two stage model. FEBS Lett 555:122–125

Fagerberg L, Jonasson K, von Heijne G, Uhlen M, Berglund L (2010) Prediction of the human membrane proteome. Proteomics 10:1141–1149

Faggad A, Darb-Esfahani S, Wirtz R, Sinn B, Sehouli J, Konsgen D, Lage H, Noske A, Weichert W, Buckendahl AC, Budczies J, Muller BM, Elwali NE, Dietel M, Denkert C (2009) Expression of multidrug resistance-associated protein 1 in invasive ovarian carcinoma: implication for prognosis. Histopathology 54:657–666

Fiedler S, Broecker J, Keller S (2010) Protein folding in membranes. Cell Mol Life Sci 67:1779–1798

Flanagan SE, Patch AM, Mackay DJ, Edghill EL, Gloyn AL, Robinson D, Shield JP, Temple K, Ellard S, Hattersley AT (2007) Mutations in ATP-sensitive K^+ channel genes cause transient neonatal diabetes and permanent diabetes in childhood or adulthood. Diabetes 56:1930–1937

Fletcher JI, Haber M, Henderson MJ, Norris MD (2010) ABC transporters in cancer: more than just drug efflux pumps. Nat Rev Cancer 10:147–156

Grant CE, Gao M, DeGorter MK, Cole SP, Deeley RG (2008) Structural determinants of substrate specificity differences between human multidrug resistance protein (MRP) 1 (ABCC1) and MRP3 (ABCC3). Drug Metab Dispos 36:2571–2581

Haimeur A, Conseil G, Deeley RG, Cole SP (2004) The MRP-related and BCRP/ABCG2 multidrug resistance proteins: biology, substrate specificity and regulation. Curr Drug Metab 5:21–53

Hedin LE, Ojemalm K, Bernsel A, Hennerdal A, Illergard K, Enquist K, Kauko A, Cristobal S, von Heijne G, Lerch-Bader M, Nilsson I, Elofsson A (2010) Membrane insertion of marginally hydrophobic transmembrane helices depends on sequence context. J Mol Biol 396:221–229

Hipfner DR, Almquist KC, Leslie EM, Gerlach JH, Grant CE, Deeley RG, Cole SP (1997) Membrane topology of the multidrug resistance protein (MRP). A study of glycosylation-site mutants reveals an extracytosolic NH2 terminus. J Biol Chem 272:23623–23630

Holland IB, Blight MA (1999) ABC-ATPases, adaptable energy generators fuelling transmembrane movement of a variety of molecules in organisms from bacteria to humans. J Mol Biol 293:381–399

Holland IB, Cole SPC, Kuchler K, Higgins CF (2003) ABC proteins: from bacteria to man. Academic Press, London

Hollenstein K, Dawson RJ, Locher KP (2007) Structure and mechanism of ABC transporter proteins. Curr Opin Struct Biol 17:412–418

Hunt JF, Earnest TN, Bousche O, Kalghatgi K, Reilly K, Horvath C, Rothschild KJ, Engelman DM (1997) A biophysical study of integral membrane protein folding. Biochemistry 36:15156–15176

Ito K, Olsen SL, Qiu W, Deeley RG, Cole SP (2001) Mutation of a single conserved tryptophan in multidrug resistance protein 1 (MRP1/ABCC1) results in loss of drug resistance and selective loss of organic anion transport. J Biol Chem 276:15616–15624

Jasanoff A, Fersht AR (1994) Quantitative determination of helical propensities from trifluoroethanol titration curves. Biochemistry 33:2129–2135

Jones PM, O'Mara ML, George AM (2009) ABC transporters: a riddle wrapped in a mystery inside an enigma. Trends Biochem Sci 34:520–531

Karwatsky J, Daoud R, Cai J, Gros P, Georges E (2003) Binding of a photoaffinity analogue of glutathione to MRP1 (ABCC1) within two cytoplasmic regions (L0 and L1) as well as transmembrane domains 10–11 and 16–17. Biochemistry 42:3286–3294

Kast C, Gros P (1997) Topology mapping of the amino-terminal half of multidrug resistance-associated protein by epitope insertion and immunofluorescence. J Biol Chem 272:26479–26487

Kast C, Gros P (1998) Epitope insertion favors a six transmembrane domain model for the carboxy-terminal portion of the multidrug resistance-associated protein. Biochemistry 37:2305–2313

Kerr ID, Jones PM, George AM (2010) Multidrug efflux pumps: the structures of prokaryotic ATP-binding cassette transporter efflux pumps and implications for our understanding of eukaryotic P-glycoproteins and homologues. Febs J 277:550–563

Kinosita K Jr, Kawato S, Ikegami A (1977) A theory of fluorescence polarization decay in membranes. Biophys J 20:289–305

Koike K, Oleschuk CJ, Haimeur A, Olsen SL, Deeley RG, Cole SP (2002) Multiple membrane-associated tryptophan residues contribute to the transport activity and substrate specificity of the human multidrug resistance protein, MRP1. J Biol Chem 277:49495–49503

Koike K, Conseil G, Leslie EM, Deeley RG, Cole SP (2004) Identification of proline residues in the core cytoplasmic and transmembrane regions of multidrug resistance protein 1 (MRP1/ABCC1) important for transport function, substrate specificity, and nucleotide interactions. J Biol Chem 279:12325–12336

Lakowicz JR (2006) Principles of fluorescence spectroscopy, 3rd edn. Springer, New York

Lauterwein J, Bösch C, Brown LR, Wüthrich K (1979) Physicochemical studies of the protein-lipid interactions in melittin-containing micelles. Biochim Biophys Acta 556:244–264

Le Lan C, Gallay J, Vincent M, Neumann JM, de Foresta B, Jamin N (2010) Structural and dynamic properties of juxta-membrane segments of caveolin-1 and caveolin-2 at the membrane interface. Eur Biophys J 39:307–325

Lequin O, Ladram A, Chabbert L, Bruston F, Convert O, Vanhoye D, Chassaing G, Nicolas P, Amiche M (2006) Dermaseptin S9, an alpha-helical antimicrobial peptide with a hydrophobic core and cationic termini. Biochemistry 45:468–480

Leslie EM, Deeley RG, Cole SP (2005) Multidrug resistance proteins: role of P-glycoprotein, MRP1, MRP2, and BCRP (ABCG2) in tissue defense. Toxicol Appl Pharmacol 204:216–237

Li SC, Deber CM (1994) A measure of helical propensity for amino acids in membrane environments. Nat Struct Biol 1:368–373

Liao MJ, London E, Khorana HG (1983) Regeneration of the native bacteriorhodopsin structure from two chymotryptic fragments. J Biol Chem 258:9949–9955

Liu YH, Di YM, Zhou ZW, Mo SL, Zhou SF (2010) Multidrug resistance-associated proteins and implications in drug development. Clin Exp Pharmacol Physiol 37:115–120

Livesey AK, Brochon JC (1987) Analyzing the distribution of decay constants in pulse-fluorimetry using the maximum entropy method. Biophys J 52:693–706

Locher KP (2009) Review. Structure and mechanism of ATP-binding cassette transporters. Philos Trans R Soc Lond B Biol Sci 364:239–245

Loe DW, Almquist KC, Deeley RG, Cole SP (1996) Multidrug resistance protein (MRP)-mediated transport of leukotriene C4 and chemotherapeutic agents in membrane vesicles. Demonstration of glutathione-dependent vincristine transport. J Biol Chem 271:9675–9682

London E, Feigenson GW (1981) Fluorescence quenching in model membranes. 1. Characterization of quenching caused by a spin-labeled phospholipid. Biochemistry 20:1932–1938

Lundin C, Kim H, Nilsson I, White SH, von Heijne G (2008) Molecular code for protein insertion in the endoplasmic reticulum membrane is similar for N(in)-C(out) and N(out)-C(in) transmembrane helices. Proc Natl Acad Sci USA 105:15702–15707

Marquez B, Van Bambeke F (2010) ABC multidrug transporters: target for modulation of drug pharmacokinetics and drug–drug interactions. Curr Drug Targets (in press)

Møller JV, le Maire M (1993) Detergent binding as a measure of hydrophobic surface area of integral membrane proteins. J Biol Chem 268:18659–18672

Montserret R, Aubert-Foucher E, McLeish MJ, Hill JM, Ficheux D, Jaquinod M, van der Rest M, Deleage G, Penin F (1999) Structural analysis of the heparin-binding site of the NC1 domain of collagen XIV by CD and NMR. Biochemistry 38:6479–6488

Pace CN, Vajdos F, Fee L, Grimsley G, Gray T (1995) How to measure and predict the molar absorption coefficient of a protein. Protein Sci 4:2411–2423

Pan CP, Barkley MD (2004) Conformational effects on tryptophan fluorescence in cyclic hexapeptides. Biophys J 86:3828–3835

Popot JL, Engelman DM (1990) Membrane protein folding and oligomerization: the two-stage model. Biochemistry 29:4031–4037

Popot JL, Engelman DM (2000) Helical membrane protein folding, stability, and evolution. Annu Rev Biochem 69:881–922

Powl AM, East JM, Lee AG (2005) Heterogeneity in the binding of lipid molecules to the surface of a membrane protein: hot spots for anionic lipids on the mechanosensitive channel of large conductance MscL and effects on conformation. Biochemistry 44:5873–5883

Rappa G, Lorico A, Flavell RA, Sartorelli AC (1997) Evidence that the multidrug resistance protein (MRP) functions as a co-transporter of glutathione and natural product toxins. Cancer Res 57:5232–5237

Rath A, Tulumello DV, Deber CM (2009) Peptide models of membrane protein folding. Biochemistry 48:3036–3045

Rees DC, Johnson E, Lewinson O (2009) ABC transporters: the power to change. Nat Rev Mol Cell Biol 10:218–227

Reiersen H, Rees AR (2000) Trifluoroethanol may form a solvent matrix for assisted hydrophobic interactions between peptide side chains. Protein Eng 13:739–743

Robey RW, To KK, Polgar O, Dohse M, Fetsch P, Dean M, Bates SE (2009) ABCG2: a perspective. Adv Drug Deliv Rev 61:3–13

Roccatano D, Colombo G, Fioroni M, Mark AE (2002) Mechanism by which 2,2,2-trifluoroethanol/water mixtures stabilize secondary-structure formation in peptides: a molecular dynamics study. Proc Natl Acad Sci USA 99:12179–12184

Rosenberg MF, Oleschuk CJ, Wu P, Mao Q, Deeley RG, Cole SP, Ford RC (2010) Structure of a human multidrug transporter in an inward-facing conformation. J Struct Biol 170:540–547

Rothnie A, Conseil G, Lau AY, Deeley RG, Cole SP (2008) Mechanistic differences between GSH transport by multidrug resistance protein 1 (MRP1/ABCC1) and GSH modulation of MRP1-mediated transport. Mol Pharmacol 74:1630–1640

Rouvière N, Vincent M, Craescu CT, Gallay J (1997) Immunosuppressor binding to the immunophilin FKBP59 affects the local structural dynamics of a surface β-strand: time-resolved fluorescence study. Biochemistry 36:7339–7352

Sharom FJ (2008) ABC multidrug transporters: structure, function and role in chemoresistance. Pharmacogenomics 9:105–127

Sillen A, Engelborghs Y (1998) The correct use of "average" fluorescence parameters. Photochem Photobiol 67:475–486

Situ D, Haimeur A, Conseil G, Sparks KE, Zhang D, Deeley RG, Cole SP (2004) Mutational analysis of ionizable residues proximal to the cytoplasmic interface of membrane spanning domain 3 of the multidrug resistance protein, MRP1 (ABCC1): glutamate 1204 is important for both the expression and catalytic activity of the transporter. J Biol Chem 279:38871–38880

Stanley AM, Fleming KG (2008) The process of folding proteins into membranes: challenges and progress. Arch Biochem Biophys 469:46–66

Szabo AG, Rayner DM (1980) Fluorescence Decay of Tryptophan Conformers in Aqueous-Solution. J Am Chem Soc 102:554–563

Tortech L, Jaxel C, Vincent M, Gallay J, de Foresta B (2001) The polar headgroup of the detergent governs the accessibility to water of tryptophan octyl ester in host micelles. Biochim Biophys Acta 1514:76–86

Tusnady GE, Sarkadi B, Simon I, Varadi A (2006) Membrane topology of human ABC proteins. FEBS Lett 580:1017–1022

Vincent M, Gallay J (1991) The interactions of horse heart apocytochrome c with phospholipid vesicles and surfactant micelles: time-resolved fluorescence study of the single tryptophan residue (Trp-59). Eur Biophys J 20:183–191

Vincent M, Brochon JC, Merola F, Jordi W, Gallay J (1988) Nanosecond dynamics of horse heart apocytochrome c in aqueous solution as studied by time-resolved fluorescence of the single tryptophan residue (Trp-59). Biochemistry 27:8752–8761

Vincent M, Gallay J, Demchenko AP (1995) Solvent relaxation around the excited state of indole: analysis of fluorescence lifetime distributions and spectral shift. J Phys Chem 99:14931–14941

Vincent M, Gilles AM, Li de la Sierra IM, Briozzo P, Barzu O, Gallay J (2000) Nanosecond fluorescence dynamic Stokes shift of tryptophan in a protein matrix. J Phys Chem B 104:11286–11295

Vincent M, Gallay J, Jamin N, Garrigos M, de Foresta B (2007) The predicted transmembrane fragment 17 of the human multidrug resistance protein 1 (MRP1) behaves as an interfacial helix in membrane mimics. Biochim Biophys Acta 1768:538–552

Ward A, Reyes CL, Yu J, Roth CB, Chang G (2007) Flexibility in the ABC transporter MsbA: alternating access with a twist. Proc Natl Acad Sci USA 104:19005–19010

Westlake CJ, Cole SP, Deeley RG (2005) Role of the NH2-terminal membrane spanning domain of multidrug resistance protein 1/ABCC1 in protein processing and trafficking. Mol Biol Cell 16:2483–2492

White SH, von Heijne G (2005) Transmembrane helices before, during, and after insertion. Curr Opin Struct Biol 15:378–386

White SH, Wimley WC (1999) Membrane protein folding and stability: physical principles. Annu Rev Biophys Biomol Struct 28:319–365

Whitmore L, Wallace BA (2004) DICHROWEB, an online server for protein secondary structure analyses from circular dichroism spectroscopic data. Nucleic Acid Res 32:W668–W673

Whitmore L, Wallace BA (2008) Protein secondary structure analyses from circular dichroism spectroscopy: methods and reference databases. Biopolymers 89:392–400

Willis KJ, Neugebauer W, Sikorska M, Szabo AG (1994) Probing α-helical secondary structure at a specific site in model peptides via restriction of tryptophan side-chain rotamer conformation. Biophys J 66:1623–1630

Yang Y, Chen Q, Zhang JT (2002) Structural and functional consequences of mutating cysteine residues in the amino terminus of human multidrug resistance-associated protein 1. J Biol Chem 277:44268–44277

Zhang DW, Cole SP, Deeley RG (2002) Determinants of the substrate specificity of multidrug resistance protein 1: role of amino acid residues with hydrogen bonding potential in predicted transmembrane helix 17. J Biol Chem 277:20934–20941

Zhang DW, Nunoya K, Vasa M, Gu HM, Cole SP, Deeley RG (2006) Mutational analysis of polar amino acid residues within predicted transmembrane helices 10 and 16 of multidrug resistance protein 1 (ABCC1): effect on substrate specificity. Drug Metab Dispos 34:539–546